

# Scratch Testing Performance of Thermally Sprayed WC-10Co-4Cr and Al<sub>2</sub>O<sub>3</sub> Coated CA6NM Steel

Sanjeev Kumar<sup>1</sup> · Sanjeev Bhandari<sup>2</sup> · Manpreet Kaur<sup>2</sup>

<sup>1</sup>IKGPTU Kapurthala, India.

<sup>2</sup>Baba Banda Singh Bahadur Engineering College, Fatehgarh Sahib, India.

## ABSTRACT

In the present investigation, the scratch testing performance of the D-gun spray WC-10Co-4Cr and Al<sub>2</sub>O<sub>3</sub> coatings deposited on CA6NM steel has been studied. The enhancements in mechanical properties were analyzed by conducting various tests such as microstructural observations, microhardness, and scratch tests. The scratch tests were performed by moving a Diamond Rockwell C indenter across a specimen's surface under constant and progressive increasing loads. The scratch tests revealed substantial information about the quality of the coatings and their scratch resistance properties. A lower coefficient of friction (CoF) values was obtained on Al<sub>2</sub>O<sub>3</sub> coated steel in comparison with the WC-10Co-4Cr coating. This was mainly attributed to the higher apparent scratch hardness values of the WC-10Co-4Cr coating. The various signatures such as microcracking and pull-outs in the scratch tracks of both coatings were observed. The Al<sub>2</sub>O<sub>3</sub> coating exhibited a higher incidence of fractured regions along the edges of the scratch tracks.

©The Indian Thermal Spray Association, INSCIENCEIN. 2024. All rights reserved

## ARTICLE HISTORY

Received 14-07-2024

Revised 02-09-2024

Accepted 04-09-2024

Published 23-09-2024

## KEYWORDS

Scratch Testing  
Coefficient of friction  
Traction force  
Coatings  
Scratch width  
Apparent Scratch  
Hardness

## Introduction

Modern coating techniques enhance the performance and durability of engineering components [1-2]. Effective coating methods can mitigate these issues by enhancing the wear resistance and durability of critical components and thermal spray methods offer a versatile approach to creating a diverse range of coatings and protective layers [3]. Thermal spray coating materials play a pivotal role across several advanced technology sectors due to their unique properties and processing versatility and involves using a heat source to melt metallic and nonmetallic powders, which are then sprayed at high velocity onto a substrate to form a dense, protective coating. This process, widely used to protect components from wear, corrosion, and thermal shock, requires precise control of equipment settings, such as power, powder feed rate, and spray distance. Coating properties like porosity, adhesion, and roughness are influenced by the shape and bonding of splats—individual molten droplets that accumulate on the substrate. Substrate temperature plays a crucial role in determining splat shape and, consequently, the coating's overall quality [4]. Oxidation during the processing of thermally sprayed metal coatings significantly affects their phase composition, microstructure, and properties, ultimately impacting performance. Oxides within the coating alter the material properties compared to the bulk material [5]. The detonation gun (D-gun) spray process stands out among the techniques used for applying thin coatings due to its remarkable performance attributes. This process delivers coatings characterized by excellent adhesion, minimal porosity, and surfaces with compressive residual stresses, the D-gun process ensures low oxide content and high inters plat strength, which contribute to the overall durability and effectiveness of the coatings [6-9]. These qualities make the D-gun spray process particularly valuable in demanding applications where

high-quality coatings are essential for enhancing material performance and longevity. In the D-gun spray process, powdered materials are introduced into a rapidly moving stream of combustion products generated by a detonation wave traveling through a water-cooled barrel. As this high-energy mixture exits the barrel, it strikes a designated substrate. The intense heat and force cause the particles to adhere to the surface, forming a layered structure of bonded platelets. This process results in coatings with strong adhesion, minimal porosity, and high strength, making it ideal for applications requiring durable and high-performance thin films [10]. Ceramic materials, such as nickel-chromium, tungsten carbide, and aluminum oxide, are highly valued for their wear resistance, particularly when applied as coatings. These coatings are typically produced using atmospheric plasma spraying (APS). APS generated the high temperatures needed to melt ceramic powders, which have high melting points. The molten ceramic material can then deform and adhere properly to the surface being coated, forming a durable, wear-resistant layer. This process is cost-effective and utilizes readily available materials, making it a popular choice in various industrial applications where wear resistance is critical [11]. Compared to high-velocity thermal-sprayed coatings, plasma-sprayed coatings typically have higher porosity and greater brittleness [12,13]. High-velocity combustion spraying techniques, such as D-gun spraying, create coatings with tighter interlamellar contacts and lower porosity, resulting in higher hardness levels, especially for oxide coatings [14,15]. The scratch test remains a simple and effective method for evaluating coating adhesion by simulating real-world abrasion, and higher friction coefficients indicate more wear, while lower values suggest better lubrication and extended coating lifespan. During concrete crushing in cement plants, rotating shafts face unavoidable stresses, leading to mechanical interactions

that often cause scratches and wear on material processing machinery components, as illustrated in Fig. 1.

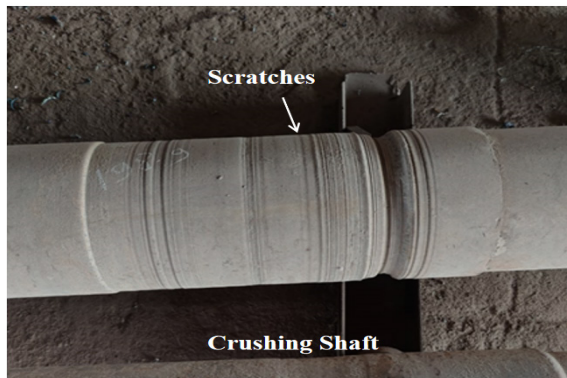


**Figure 1:** Scratches on the crusher shaft in one of the manufacturing plants

Al<sub>2</sub>O<sub>3</sub> (aluminum oxide) coatings are highly valued in various industrial applications due to their outstanding mechanical and chemical properties. These coatings are characterized by their high hardness, excellent wear resistance, and ability to withstand high temperatures, making them ideal for protecting surfaces exposed to harsh conditions [12-15]. WC-10Co-4Cr, a composite material made up of tungsten carbide (WC) particles embedded in a matrix of cobalt (Co) and chromium (Cr). This composition is known for their excellent wear resistance, hardness, and corrosion resistance, making them suitable for a variety of industrial applications [16,17]. The study investigates the scratch testing performance of D-Gun sprayed Al<sub>2</sub>O<sub>3</sub> and WC-10Co-4Cr Coated CA6NM stainless steel specimens to analysis problem basis the Scratch test.

## Experimental

### Substrate Material

CA6NM stainless steel (ASTM 743-grade) is commonly used as a substrate for coatings, particularly in the energy sector for runners, underwater components in hydro turbines, and cement plant shafts due to its excellent hardness and corrosion resistance. The chemical composition and mechanical properties of CA6NM steel are detailed in Tables 1 and 2, respectively. The steel was formed into rectangular specimens with dimensions of 60 mm in length, 60 mm in breadth, and 10 mm in thickness.

**Table 1:** Chemical Composition of CA6NM (ASTM A743-grade) steel

Grade	C	Mn	Cr	Mo	Ni	Fe
CA6NM	0-.06	0-1	11.5-14	0.4-1	3.5-4.5	Balance

**Table 2:** Mechanical Properties of CA6NM (ASTM A743-grade) steel

Grade	Tensile Strength (ksi)	Tensile Strength (MPa)	Yield Strength (ksi)	Elongation (%)	Hardness (Brinell)
CA6NM	≈135	≈931	≈80	≈15	≈269

### Deposition of Coatings

Al<sub>2</sub>O<sub>3</sub> and WC-10Co-4Cr powders were used as feedstock materials for coatings in this study due to their superior hardness, wear and corrosion resistance, thermal stability,

and ability to protect components in challenging environments. These materials are widely utilized in the aerospace, automotive, oil and gas, and power generation industries. Table 3 shows the specifications provided by the manufacturer. Firstly, rectangular steel specimens were grit-blasted with 60-mesh alumina grit to improve the adhesion between the coating and the substrate. The air pressure used for the blasting process was around 0.6 MPa. The D-gun spray method was then used to coat the samples, and it was made available by SVX Powder M Surface Engineering Pvt. Ltd. in Noida, India. The specified procedure parameters shown in Table 4 were used to apply the coatings.

Al<sub>2</sub>O<sub>3</sub> particles are found to have angular morphology figure 2 (a). The EDS analysis at different locations also confirms the presence of the mainly O (12.7 %) and Al (87.3 %) in the angular alumina particles 2 (b). The SEM morphology of the WC-10Co-4Cr powder is shown in Figure 3 (a). Most of the particles have a spherical morphology. The EDS analysis has confirmed the presence of W, Co, Cr and C in the feedstock powder Figure 3 (b).

**Table 3:** Characteristics of Al<sub>2</sub>O<sub>3</sub> and WC-10Co-4Cr powders

Powder	Chemical composition (wt %)	Morphology	Make	Particle Shape	Powder Size
Al <sub>2</sub> O <sub>3</sub>	SiO <sub>2</sub> max.0.2 %	Powder Fusion	H.C. Strack	Regular	47/25 μm
	Fe <sub>2</sub> O <sub>3</sub> max.0.4 %				
	Na <sub>2</sub> O max.0.2 %				
	Al <sub>2</sub> O <sub>3</sub> balance				
	Co 9-11% Cr 3-5 % C 5-6 %				
WC-10Co-4Cr	Fe max 0.3 % O max 0.2 % W balance	Agglomerated Sintered	H.C. Strack	Spherical	- 88+17 μm

The investigation into the surface characteristics of these applied coatings was then observed using a scanning electron microscope (JEOL JSM-6610LV). To analyze the coatings further, particularly in cross-section, a slow-speed diamond cutter was used to minimize the risk of the coating separating from the substrate during sectioning. Afterward, the prepared specimens were mounted and meticulously polished.

**Table 4:** Process parameters for D-gun spray process

Parameters	Al <sub>2</sub> O <sub>3</sub> coating	WC-10Co-4Cr coating
Acetylene flow rate (C <sub>2</sub> H <sub>2</sub> )	1,920 SLPH	2,240 SLPH
Pressure	0.14 MPa	0.14 MPa
Nitrogen flow rate (N <sub>2</sub> )	800 SLPH	720SLPH
Pressure	0.4 MPa	0.4 MPa
Oxygen flow rate (O <sub>2</sub> )	4,800 SLPH	5,180 SPLH
Pressure	0.2 MPa	0.2 MPa
Power	450 VA	450 VA
Spray angle	90°	90°
Spray distance	200 mm	180 mm

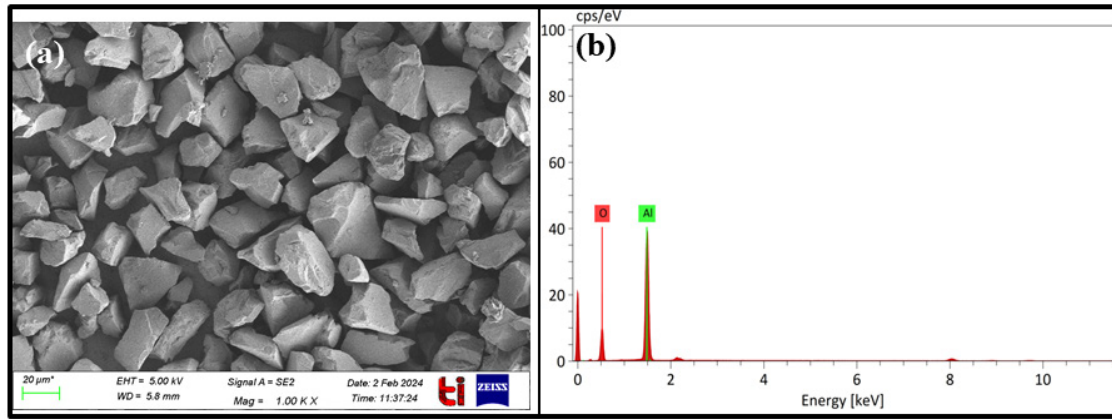


Figure 2: (a) SEM Micrograph of Al<sub>2</sub>O<sub>3</sub> powder (b) EDS analysis

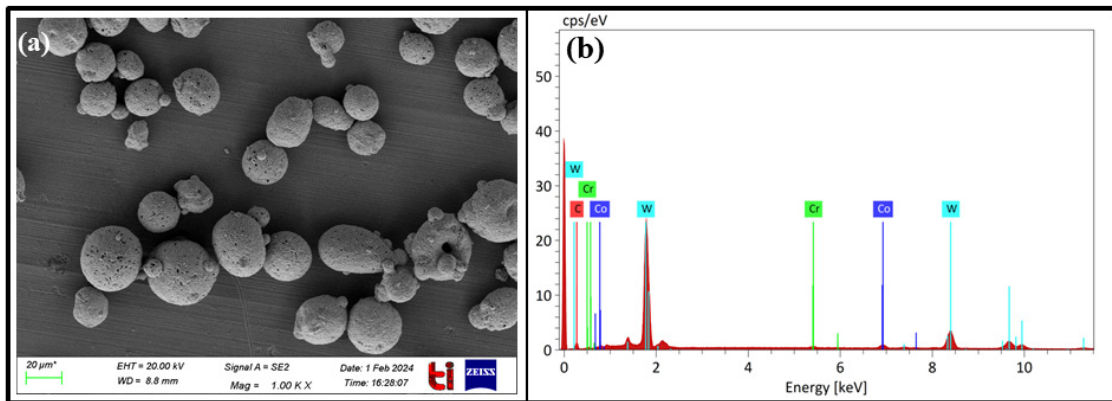


Figure 3: (a) SEM Micrograph of WC-10Co-4Cr powder (b) EDS analysis

### Scratch Testing Machine TR-101

The Blue Star stylus, a Diamond Rockwell C with a tip radius of 200 microns, is the typical indent (stylus) used for scratch testing (figure 4). It is positioned with a vice height of 240 mm from the floor, and the indenter itself is situated 250 mm above the floor. The scratch tester frame is made of 4 plates joined at edges with a vertical column mounted on the back side, the frame is supported on 4 numbers of anti-vibration pads at corners. The vertical column is for mounting motor assembly for z axis movement.

A stepper motor is mounted in vertical direction on this vertical column with motor shaft pointing towards ground, this motor rotates a screw rod coupled to it, the rotation causes a screw rod nut to raise or lower along the z axis, a compound transducer housing is screwed to the top of the screw rod nut to move along with it. The compound transducer is covered and mounted inside a housing with only the terminals protruding out and connected to socket; signals received from the sensors pass to controller through cables. An indenter holder is screwed to base of transducer unit in vertical direction, with indenter projecting below the holder, indenter is easily replaced by unscrewing from holder. The z axis screw rod is covered for exposure to dust, on the axis end limits two proximity sensors are mounted at top and bottom to prevent over travel along z axis. The x axis movement is motor drive through a second screw rod and nut arrangement, motor drives screw rod through a belt drive, the rotation of screw rod causes nut to move linearly with compound slide and vice, the x axis movement is for scratching the specimen surface by indenter, the maximum travel length is 50 mm.

The specimen size 60 x 60 x 10 mm<sup>3</sup> and is secured using a mechanical vice clamping mechanism. The recommended

loading rates are available in both constant and ramp types, with options for 0.2, 0.5, 10, and 20 N/mm. These loading rates can be applied within two specified ranges: 1) 20 to 200N, and 2) in a unidirectional manner with a stroke length ranging from 1 to 50 mm, adjustable in 1 mm increments. Tractional force during testing is measured using a 200N compound load cell, with a minimum detection limit of 20N and a maximum capacity of 200N. The indenter (stylus) can move at various speeds, ranging from 0.1 to 5 mm/sec, with increment options of 0.1, 0.2, 0.5, 1, 2, 3, 4 and 5 mm/sec. The movement occurs along the X-axis with a motorized travel range of 0 to 50 mm, along the Y-axis with manual micrometer adjustment of 0 to 5 mm, and along the Z-axis with motorized loading spanning 75 mm. Single-scratching was made on the WC-10Co-4Cr and Al<sub>2</sub>O<sub>3</sub> coatings. For all the tests, the scratching length was 5 mm kept.



Figure 4: Experimental setup

### Surface Roughness, Microhardness, Porosity and Fracture Toughness Measurements

The surface roughness of the specimen has an influence on the outcome of scratch testing. The surface texture of coatings, on the other hand, is shaped by several factors, including the characteristics of powder particles and spray conditions. These spray conditions involve variables such as the type of gas used as fuel, temperature, and the velocity of the spray. To assess the surface roughness of coated and uncoated specimens, we employed a surface roughness tester (Make: Mitutoyo, Model: Surf test SJ 400) on the as-sprayed, eroded, and coated surfaces. The test results three different values at three different locations on the specimen in  $\mu\text{m}$ . In thermal-sprayed coatings, the presence of porosity or voids within the microstructure is significant, as it affects various coating properties such as inter-splat bonding, microhardness, and crack propagation. Consequently, image analysis software (Envision 3.0) was utilized to quantify the apparent porosity in the as-sprayed coatings on mirror-polished cross-sections. To determine the coating's fracture toughness, an indentation method, measuring the length of cracks originating from the corners of Vickers indentation diagonals under 300 grams for a dwell time of 20s was used.

**Table 5:** Variation of Micro Hardness for the coated and uncoated specimens

CA6NM Steel	CA6NM + WC-10Co-4Cr	CA6NM + Al <sub>2</sub> O <sub>3</sub>
330 ± 20 HV	607.43 ± 28.53	783.98 ± 36.58

## Results and Discussion

### Characterization

Surface morphology of as-sprayed WC-10Co-4Cr coating on CA6NM is shown in Figure 5. The coating, in general, has a nearly uniform surface microstructure consisting of interlocked splats. The coating seems to have the presence of fine WC grains dispersed in the matrix. The WC grains appear as round white particles, whereas very dark small round spots are micro-pores. It is believed that Co-Cr binder matrix exhibits different grey shades, and the regions of higher brightness indicate the dissolution of WC into the binder phase.

The SEM micrograph of Al<sub>2</sub>O<sub>3</sub> coating which is characterized by variations in grey level contrast due to presence of different region (melted and partially melted) and variation in powder particle size is shown in Figure 6. The micrograph of the surface of the coating also indicates the presence of micropores at some places, in a well-formed splat-like microstructure. Figures 7 and 8 show the cross-sectional SEM along with Energy-dispersive X-ray spectroscopy (EDS) report of WC-10Co-4Cr and Al<sub>2</sub>O<sub>3</sub> coatings respectively. The coating-substrate interface is by and large, intact and continuous. The coating, in general have splat like morphology formed in a lamellar fashion. The porosity of coatings coating was found to be less than 2 %. Vickers microhardness was taken at different locations following ISO-6507 standard with measurements taken at various points using a 100g load and 20s dwell time. Average values were calculated along with standard error accounting for deviations from these averages. The summarized results in table 5, the hardness values for each material system. CA6NM exhibited hardness of 330 ± 20 Hv, while the CA6NM + WC-10Co-4Cr has 607.43 ± 28.53 and CA6NM + Al<sub>2</sub>O<sub>3</sub> exhibited 783.98 ± 36.58. CA6NM + Al<sub>2</sub>O<sub>3</sub> displayed 2.37 times higher hardness than CA6NM steel

following CA6NM + WC-10Co-4Cr displayed 1.29 times better than the CA6NM steel.

### Scratch Tests Analysis

A mechanical system, such as a block on a horizontal surface is used to understand the relationship between normal force, tractional force, and CoF with reference to stroke length. Here is a succinct justification: Standard Force (N): The perpendicular force that an indenter applies to a surface in contact with it is known as the normal force. When a block is supported by a horizontal surface, the normal force is equal to the object's weight (mg), where "m" denotes the block's mass and "g" denotes the acceleration brought on by gravity. Tractional Force (F) is the force that resists an object's motion or imminent motion and is parallel to the surface. It relies on a number of variables, including the normal force and the coefficient of friction. A common formula for tractional force is  $F = \mu N$ , where F stands for tractional force,  $\mu$  for CoF, and N for normal force.

To know the extent of surface damage on the coatings during the scratching under different loads, scratch testing has been performed under loads of 20N, 50N, 100N, 150N, 200N and Ramp Load 40-200N with constant and progressively increasing load. There are several factors such as surface roughness, scratch speed, load and coating properties that can cause variation in the CoF values along the scratch length during scratch testing. To understand the tribological and mechanical behaviour of coated samples, the graphs of CoF versus scratch length during the scratch test under constant and progressively increasing loads are drawn (Figures 10-14,18). Typically, the graph shows how the CoF changes as the scratch length increases during the test. At the beginning of each scratch test, the CoF is relatively low. This may be due to the elasticity of the coated samples. In the beginning of a test, when the indenter first contacts the coating surface, there is an increase in the CoF. The initial peak in CoF may be attributed to the start of the material deformation. As the scratching continues, the CoF fluctuate as the indenter plough through the coating material. During this stage, the CoF values may vary depending on the local microstructure, hardness variations, and the presence of hard particles or phases within the coating. In regions where cracks occur within the coating, the CoF values may change abruptly due to changes in contact area, frictional forces, and material removal mechanisms. Fracture events can lead to fluctuations in CoF as the indenter encounters different resistance levels along the scratch length. Table 6 shows the observed average CoF values under different loads of the coatings and (figure 9) shows the variation of average CoF for Al<sub>2</sub>O<sub>3</sub>, WC-10Co-4Cr coatings and CA6NM steel at 20N,50N,100N,150N,200N and Ramp Load of 40-200N.

The critical loads increase with the hardness and toughness of the substrate materials, coating has been influenced by the coefficient of friction [18]. Simulations are used to analysis the friction and wear behavior of asperity-asperity contact during sliding. The CoF increased with the number of scratches. [19]. The CoF was measured to analyze the cold spray deposits under progressive and constant loading circumstances. The indenter was moved across a 4 mm scratch distance with a 40N force for the continuous load test. According to the results, the as-received powder deposit exhibited the lowest CoF (~0.19) of all the samples. S3HT NAB, on the other hand, exhibited a higher CoF

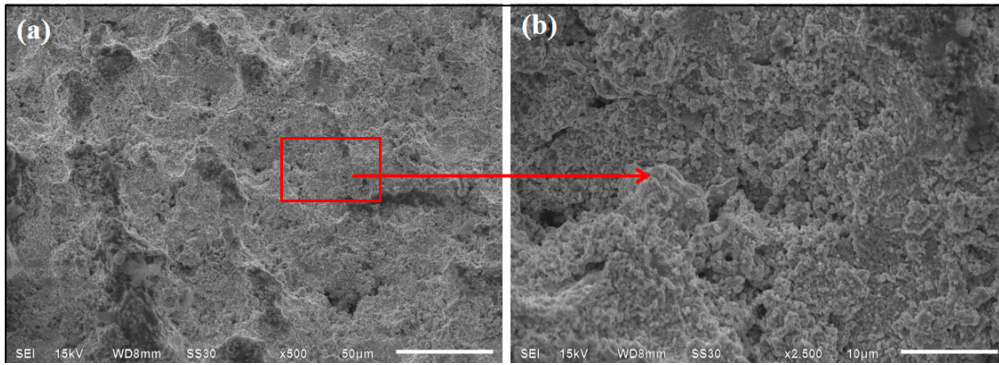


**Figure 5:** Surface SEM analysis of the D-gun sprayed WC-10Co-4Cr coating on CA6NM steel in as-sprayed condition

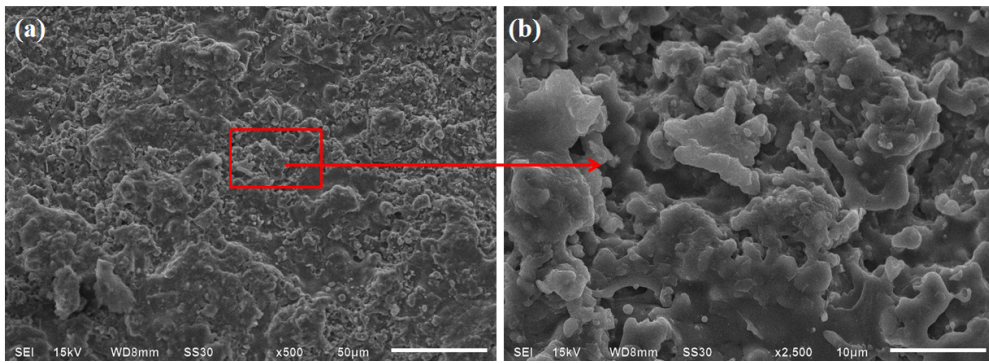


**Figure 6:** Surface SEM analysis of the D-gun sprayed Al<sub>2</sub>O<sub>3</sub> coating on CA6NM steel in as-sprayed condition

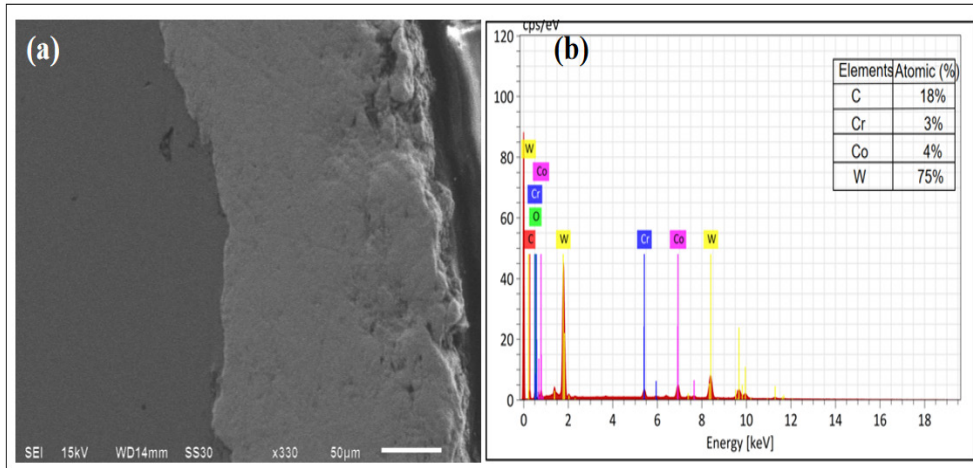


**Figure 7:** Cross-sectional SEM along with EDS analysis of the D-gun sprayed WC-10Co-4Cr coating on CA6NM steel in as-sprayed condition

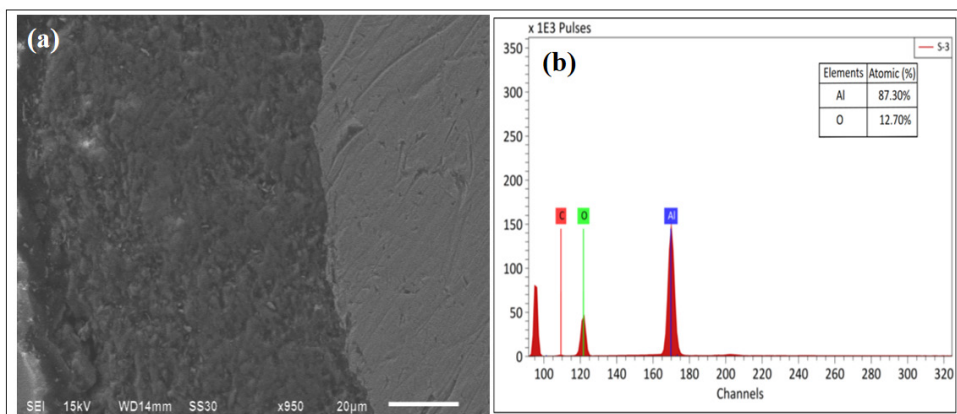


**Figure 8:** Cross-sectional SEM along with EDS analysis of the D-gun sprayed Al<sub>2</sub>O<sub>3</sub> coating on CA6NM steel in as-sprayed condition

(~0.43) among the heat-treated powder deposits, whereas S2HT NAB had a lower CoF (~0.25). Under progressive loading, a similar pattern was seen, with the load increasing by 20 N/mm over a distance of 4 mm, culminating in a maximum of 100N. The level of inter-splat bonding within the deposits was revealed by the indenter's deeper penetration made possible by this sequential loading [20].

**Table 6:** The average values of CoF for coated and uncoated specimens

Load (N)	WC-10Co-4Cr	Al <sub>2</sub> O <sub>3</sub>	Substrate
20N	0.201	0.166	0.227
50N	0.241	0.189	0.246
100N	0.305	0.226	0.279
150N	0.271	0.230	0.289
200N	0.198	0.176	0.179
Ramp Load 40-200N	0.266	0.176	0.284

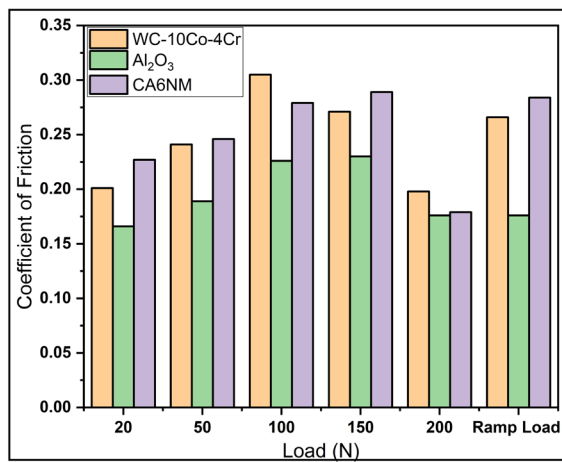


**Figure 9:** Variation of Average CoF for Al<sub>2</sub>O<sub>3</sub>, WC-10Co-4Cr coatings and CA6NM steel at 20N, 50N, 100N, 150N, 200N and Ramp Load of 40-200N

Under all testing loads, Al<sub>2</sub>O<sub>3</sub> coating has lower CoF as compared to WC-10Co-4Cr coating. Al<sub>2</sub>O<sub>3</sub> coatings are more resistant to scratch/deformations resulting in reduced penetrations/interactions with the indenter. More deformations and adhesion load results in higher values of CoF values for WC-10Co-4Cr coating. The presence of pores can also affect the contact area between the coating and the indenter. With increased porosity, the surface area available for the contact is reduced resulting in higher pressure on the remaining contact points. This increased pressure can lead to strong interactions between the coating and the indenter, resulting in higher friction. Coatings are characterized by unmelted regions, molten regions, pores, and the hardness of these phases (metallic and ceramics). Variations in these characteristics along the scratch length can result in differences in the CoF. Coating fracture toughness and its response time to strain and damage, including scratches, should be considered while assessing its performance. Therefore, it is vital to examine and ascertain fracture toughness in connection to scratch activity patterns. Increased resistance to crack initiation and propagation is often represented by a higher fracture toughness, which may have an impact on the coating's ability to withstand scratches and maintain structural integrity under mechanical stress.

Understanding this relationship facilitates the prediction and improvement of coating stability and robustness in a variety of situations.

When the surface experiences severe deformation or cracking, the normal load value decreases. Initially, in Figure 10, the normal load 20N remains constant, but as the indenter progresses through the coating, it fluctuates before stabilizing once again, with minor variations. This normal load is referred to as the critical load and is used to calculate the adhesive force. In Figure 10, at a stroke length of 1 mm, there is a sudden surge in the traction force and CoF, indicating that the coating shows cracks in the scratch path. The average value of CoF for Al<sub>2</sub>O<sub>3</sub> coating is 0.166 for scratch number 1 at a scratch length of 5 mm, 0.201 for WC-10Co-4Cr and 0.227 for CA6NM steel as shown in the table 6.

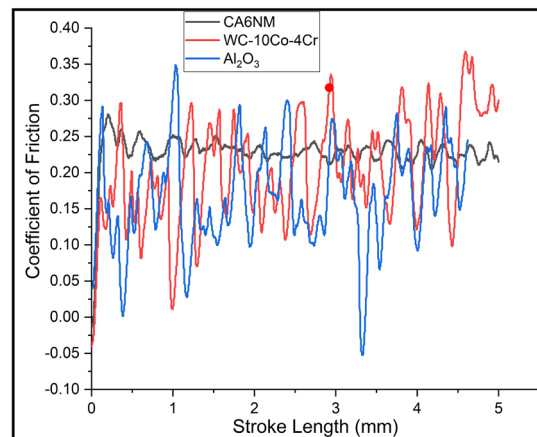


**Figure 10:** Variation of CoF along the stroke length (5mm) for Al<sub>2</sub>O<sub>3</sub>, WC-10Co-4Cr Coating and CA6NM steel substrate under a load of 20 N with scratch velocity of 0.1 mm/sec

The CoF varies, as seen in Figure 10. The initial load in this case is 20N, and once the coating reaches a length of 1 mm, there is an abrupt increase in the value of the traction force, which shows increase in CoF and cracks in coating. Additionally, it displays how the CoF varies.

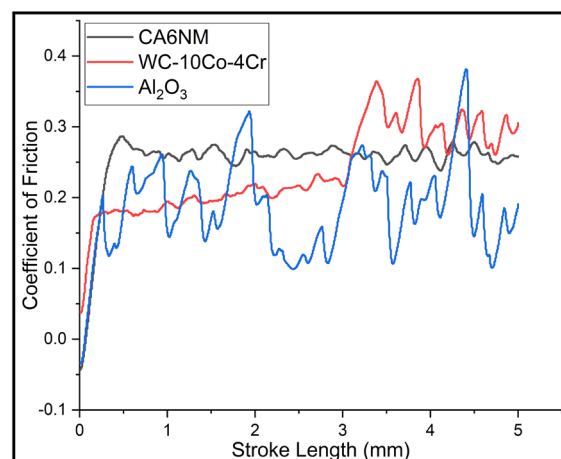


**Figure 11:** Variation of CoF along the stroke length (5mm) for Al<sub>2</sub>O<sub>3</sub>, WC-10Co-4Cr Coating and CA6NM steel substrate under a load of 50 N with scratch velocity of 0.1 mm/sec

Figure 11 displays the usual CoF and stroke in the sample as functions of the typical load. This figure demonstrates how the CoF rises together with applied force and stylus

penetration into the coating-substrate system. Because the stylus deeply penetrates the coating system even at low loads, there is no area where the CoF is independent of the applied load. The scratch reaction of every coating-substrate system was dominated by plastic deformation and a buildup of substrate material surrounding the scratch.

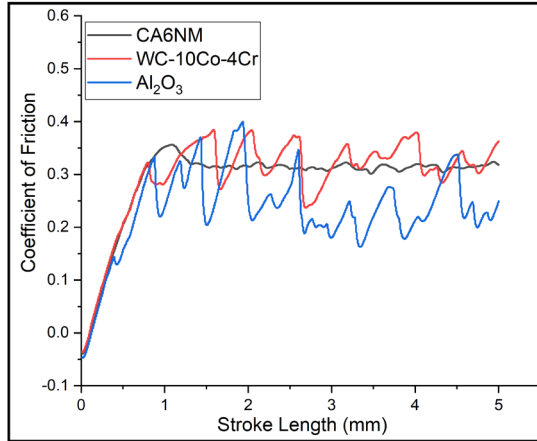


**Figure 12:** Variation of CoF along the stroke length (5mm) for Al<sub>2</sub>O<sub>3</sub>, WC-10Co-4Cr Coating and CA6NM steel substrate under a load of 100N with scratch velocity of 0.1 mm/sec

The variation of CoF along a 5mm stroke length (figure 12) for Al<sub>2</sub>O<sub>3</sub>, WC-10Co-4Cr coating, and CA6NM steel substrate under a 100N load with a scratch velocity of 0.1 mm/sec is influenced by the inherent properties of each material and their interactions under these specific conditions. Initially, the CoF is typically higher due to the interaction of asperities and the breaking through of surface oxide layers. As the stroke progresses, the CoF for Al<sub>2</sub>O<sub>3</sub> may show fluctuations due to its brittle nature, potentially causing micro-cracking and debris formation. In contrast, WC-10Co-4Cr coating tends to maintain a relatively stable CoF because of its high hardness and toughness, which provide consistent wear resistance. For the CA6NM steel substrate, the CoF might initially be higher due to metallic surface interactions and then stabilize as the surface smoothens. Towards the end of the stroke, all materials may exhibit an increased CoF due to debris accumulation, surface roughening from wear, and potential surface fatigue. Specifically, CA6NM steel could experience surface hardening, further contributing to the rise in CoF. Overall, the CoF varies dynamically along the stroke length, with initial and final increases and relative stabilization in the middle, dictated by the wear mechanisms, material properties, and surface conditions of each material.

Under a load of 150N (figure 13) with a scratch velocity of 0.1 mm/sec, the CoF along a 5mm stroke length varies distinctly for Al<sub>2</sub>O<sub>3</sub>, WC-10Co-4Cr coating, and CA6NM steel substrate. For Al<sub>2</sub>O<sub>3</sub>, the CoF starts high due to initial asperity interactions and may exhibit significant fluctuations throughout the stroke due to its brittle nature, leading to micro-cracking and debris generation. WC-10Co-4Cr coating, known for its exceptional hardness and toughness, tends to maintain a relatively stable CoF along the stroke, with minor variations resulting from slight wear and debris accumulation. In the case of the CA6NM steel substrate, the CoF is initially high due to metallic surface interactions and may stabilize somewhat in the middle of the stroke as the surface smoothens.

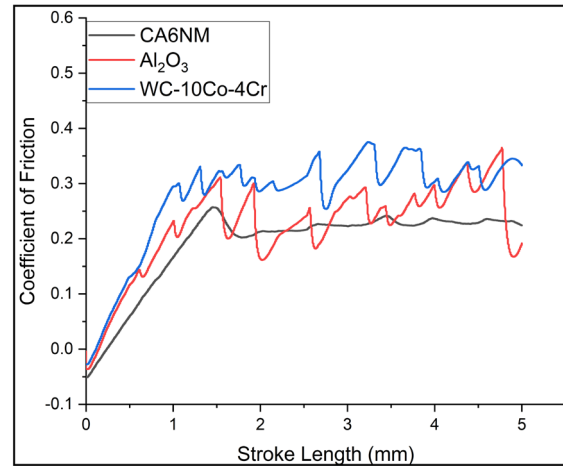


**Figure 13:** Variation of CoF along the stroke length (5mm) for Al<sub>2</sub>O<sub>3</sub>, WC-10Co-4Cr Coating and CA6NM steel substrate under a load of 150N with scratch velocity of 0.1 mm/sec

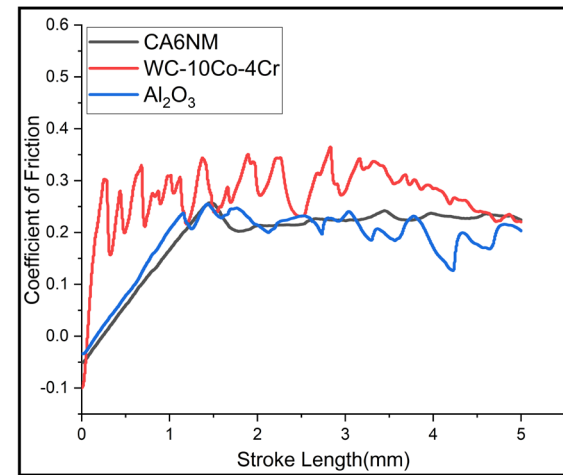


**Figure 14:** Variation of CoF along the stroke length (5mm) for Al<sub>2</sub>O<sub>3</sub>, WC-10Co-4Cr Coating and CA6NM steel substrate under a load of 200N with scratch velocity of 0.1 mm/sec

### Effect of Load

The effect of load on the variation of the CoF along a 5mm stroke length for Al<sub>2</sub>O<sub>3</sub> (figure 15) under loads of 20N, 50N, 100N, 150N, and 200N with a scratch velocity of 0.1 mm/sec demonstrates a pronounced relationship between load and frictional behavior. At lower loads, such as 20N and 50N, the CoF tends to be relatively stable with minor fluctuations due to the minimal deformation and wear. As the load increases to 100N, the CoF becomes more variable, reflecting increased asperity interactions and the onset of micro-cracking in the brittle Al<sub>2</sub>O<sub>3</sub> material. At 150N, these fluctuations become more pronounced, with higher initial CoF due to asperity engagement and subsequent variations from crack propagation and debris formation. Under the highest load of 200N, the CoF exhibits significant variability along the stroke length, characterized by high initial values and frequent fluctuations due to extensive micro-cracking, debris generation, and increased surface roughening. Overall, higher loads amplify the brittle nature of Al<sub>2</sub>O<sub>3</sub>, leading to greater CoF variability and highlighting the material's sensitivity to increased mechanical stresses.

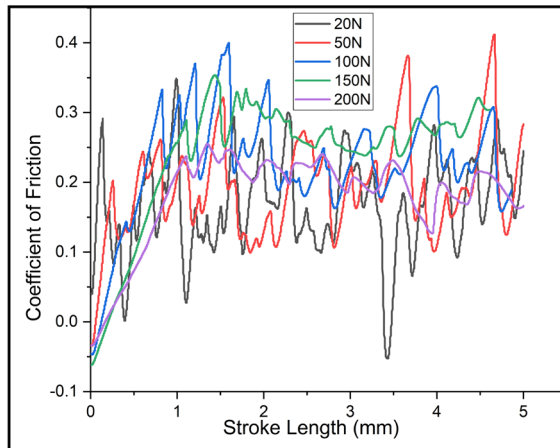


**Figure 15:** Variation of CoF along the stroke length (5mm) for Al<sub>2</sub>O<sub>3</sub> under a load of 20N, 50N, 100N, 150N and 200 N with scratch velocity of 0.1 mm/sec

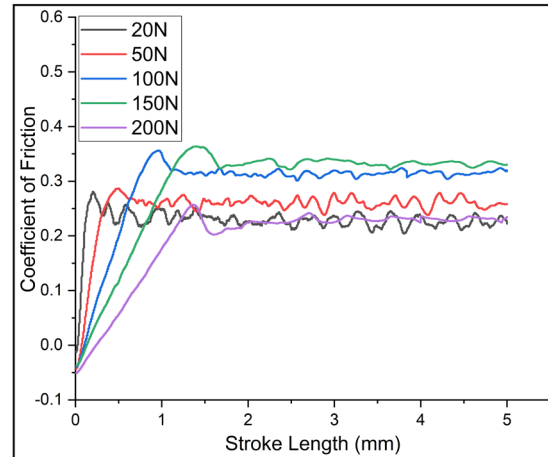


**Figure 17:** Variation of CoF along the stroke length (5mm) for CA6NM steel under a load of 20N, 50N, 100N, 150N and 200 N with scratch velocity of 0.1 mm/sec.

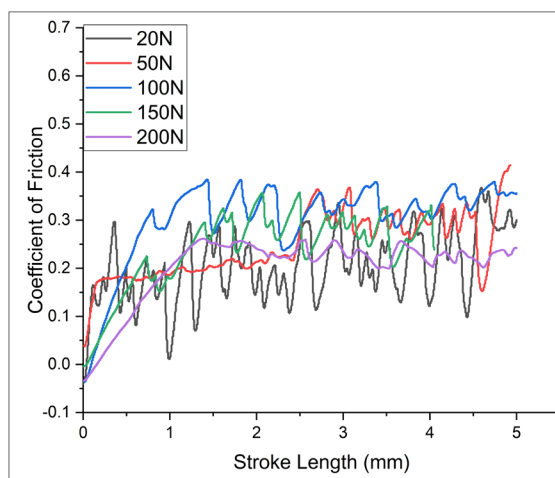


**Figure 16:** Variation of CoF along the stroke length (5mm) for WC-10Co-4Cr under a load of 20N, 50N, 100N, 150N and 200 N with scratch velocity of 0.1 mm/sec

The variation of the CoF along a 5mm stroke length (figure 16) for WC-10Co-4Cr under loads of 20N, 50N, 100N, 150N, and 200N with a scratch velocity of 0.1 mm/sec demonstrates the material's robust wear resistance and stability. At lower loads of 20N and 50N, the CoF remains relatively stable with minimal fluctuations, reflecting the coating's high hardness and toughness, which minimize wear and deformation. As the load increases to 100N, the CoF may show slight variations due to increased contact area and minor wear, but overall stability is maintained. At 150N, the CoF begins to exhibit more noticeable, yet still moderate, variations along the stroke length, primarily due to the increased mechanical stress leading to more pronounced surface interactions and slight debris formation. Under the highest load of 200N, the CoF remains relatively stable compared to other materials, though minor fluctuations become more apparent due to greater wear and debris accumulation. Overall, WC-10Co-4Cr maintains a consistently stable CoF across varying loads, underscoring its excellent wear resistance and ability to withstand increased mechanical stresses with minimal impact on frictional behavior.

The variation of the CoF along the stroke length of 5 mm for CA6NM steel (figure 17) was observed under different loads of 20N, 50N, 100N, 150N and 200N with a consistent

scratch velocity of 0.1 mm/sec. As the load increased, the CoF demonstrated a noticeable trend. At lower loads, such as 20 N, the CoF remained relatively stable along the stroke length, indicating less interaction between the steel surface and the counter material. However, as the load increased to 50 N and beyond, there was a marked increase in the CoF, with noticeable fluctuations along the stroke length. These fluctuations are likely due to the increased contact pressure causing more surface asperities to engage, leading to variations in the frictional force. At the highest load of 200 N, the CoF showed the most significant variation, suggesting that higher loads may lead to increased material deformation and wear, thereby affecting the stability of the frictional behavior. This variation highlights the sensitivity of frictional properties to applied load and the interaction between contact mechanics and material properties.

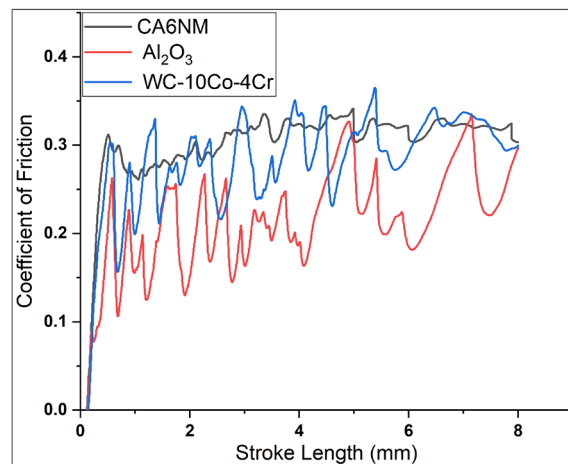


**Figure 18:** Variation of CoF along the stroke length (8mm) for CA6NM steel, Al<sub>2</sub>O<sub>3</sub> and WC-10Co-4Cr under a Ramp Load of 40-200N with scratch velocity of 0.2 mm/sec.

The variation of the CoF along the stroke length of 8 mm was studied for CA6NM steel (figure 18), Al<sub>2</sub>O<sub>3</sub>, and WC-10Co-4Cr under a ramp load ranging from 40N to 200N, with a consistent scratch velocity of 0.2 mm/sec. As the load increased progressively from 40N to 200N, each material exhibited distinct frictional characteristics. For CA6NM steel, the CoF initially showed a steady increase with the rising load, reflecting enhanced surface interactions, but began to fluctuate at higher loads, likely

due to surface deformation and wear. In the case of Al<sub>2</sub>O<sub>3</sub>, the CoF remained relatively high and stable throughout most of the stroke, indicating a strong resistance to changes in load, but showed minor variations towards the end of the stroke as the load approached its maximum, possibly due to micro-fracturing or surface plowing. WC-10Co-4Cr, known for its high hardness and wear resistance, displayed a more consistent CoF across the stroke length, even under increasing loads, which suggests effective load bearing and less susceptibility to surface damage. These differences underscore the material-dependent nature of frictional behavior under varying loads and highlight the importance of selecting appropriate materials for applications involving high load and frictional demands.

### SEM Analysis of the Scratched Coatings

As shown in figure 19, the scratch test entails moving a diamond stylus across a specimen's surface while using a normal force that is gradually increased, either continuously or in discrete increments. When a "critical normal force" is reached, a coating failure that may be seen clearly occurs. As a result, this crucial force acts as a gauge for the coating's ability to adhere.

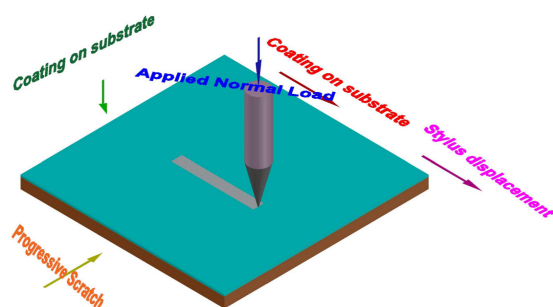


Figure 19: Mechanism of Scratch Test

Coatings are made of Al<sub>2</sub>O<sub>3</sub> and WC-10Co-4Cr are frequently employed in applications that are subject to mechanical stress. From a physical point of view, the effectiveness of any coating must be dependent on the degree of bonding between the coating and the substrate material. The efficacy of a coating, from a physical standpoint, is intricately tied to the extent of adhesion established between the coating and the underlying substrate material. Coating removal was readily detected in any of the scratch testing. The scratch pattern typically consists of several distinct zones or features that can be observed and analyzed to understand the behavior of the coating under applied stress. Here are some common features of the scratch pattern along the scratch length: 1) Incubation Zone: At the beginning of the scratch, there is an initial period where the applied load is not high enough to cause visible damage to the coating. This zone is known as the incubation zone and represents the elastic deformation of the coating before any permanent damage occurs. 2) Plastic Deformation Zone: As the applied load increases, the coating undergoes plastic deformation, resulting in the formation of a plastic groove or pile-up of material on either side of the scratch. This zone indicates the ability of the coating to deform under stress without cracking or delaminating. 3) Crack Initiation Zone: In some cases, when the applied load exceeds the critical adhesion strength of the coating-substrate interface, cracks may initiate at the edges of the scratch. These cracks can propagate along the scratch length, indicating poor adhesion or brittle behavior

of the coating. 4. Fracture Zone: With further increase in the load, the material may start to fracture or crack. Visible cracks, chipping, or flaking off of material can be observed. This zone provides insights into the material's fractured toughness and brittleness. It is particularly important for brittle materials, where the transition from plastic deformation to fracture can occur more abruptly. 5. Final Residual Zone: At the end of the scratch, there is a residual zone where material may be displaced or removed due to the scratching process. This zone can provide information about the hardness and wear resistance of the coating material. In summary, these zones help in comprehensively evaluating the material properties such as hardness, toughness, adhesion (for coatings), and wear resistance. Understanding these zones allows for better material selection and engineering design to ensure durability and performance in various applications. There is no fracture zone observed in the coated material during scratching. This absence of a fracture zone can be attributed to several factors, such as the inherent toughness and flexibility of the coating material, which allows it to deform without breaking.

After analyzing the scratched coatings under SEM (Figures 20-24), it was observed that the scratch has caused significant damage to the surface of the Al<sub>2</sub>O<sub>3</sub> coating in comparison to the WC-10Co-4Cr coating. The scratch appeared to be wider in Al<sub>2</sub>O<sub>3</sub> coating, resulting in the considerable amount of the affected zone in the Al<sub>2</sub>O<sub>3</sub> coating. The SEM images also reveal the generation of cracks along the scratch path. In addition, SEM also indicates the presence of foreign particles on the surface of coating. This may be due to the high brittleness of Al<sub>2</sub>O<sub>3</sub> coating and higher value of adhesive strength of the WC-10Co-4Cr coating.

The steps of coating cracks are shown in figure 20 and shows the alumina oxide layer on the steel substrate breaking away. There is evidence of coating cracking inside the track, where brittle failure of the coating inside the track has happened due to plastic deformation in the substrate below. The coating appears to be well bonded to the substrate, and there are no evident signs of decohesion or coating spalling.

SEM observations of Al<sub>2</sub>O<sub>3</sub> and WC-10Co-4Cr coatings fracture surfaces showed that the coating consists of sub micrometer equiaxed grains decreasing in size towards the CA6NM steel substrate. Cohesive fractures develop in the tensile stress field in the wake of the moving indenter in this failure mechanism. For loads under 20N, neither the substrate steel nor the coated CA6NM steel exhibit cracking. When compared to coating cracks, cracks in coated CA6NM steel are minor. At higher loads, the tensile cracking for both specimens become more obvious. The scratch tracks produced with a 200 N load are shown in figure 23.

Scratch tracks on and coating are seen in Figures 21,22 and 24 in SEM images (planar views), respectively. The two specimens both experienced tensile cracking. Cohesive fractures develop in the tensile stress field in the wake of the moving indenter in this failure mechanism. For loads under 20N, neither the Al<sub>2</sub>O<sub>3</sub> nor the WC-10Co-4Cr coated CA6NM steel exhibit cracking. When compared to coating cracks, cracks in WC-10Co-4Cr coated CA6NM steel are minor than Al<sub>2</sub>O<sub>3</sub> coated CA6NM steel. At higher loads, the tensile cracking for both specimens become more obvious. The scratch tracks obtained with a 200N load are shown in

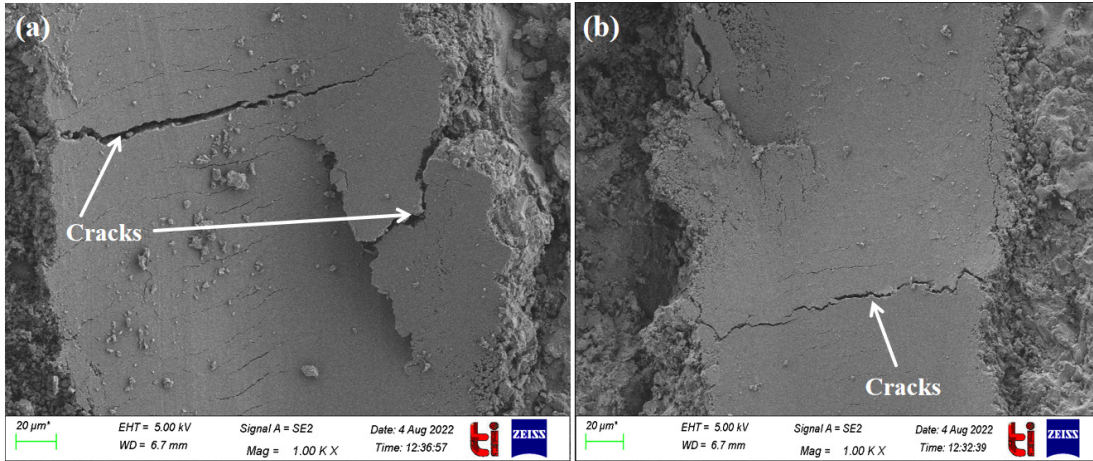


Figure 20: SEM micrographs of Al<sub>2</sub>O<sub>3</sub> coating at (a) 50N (b) 150N

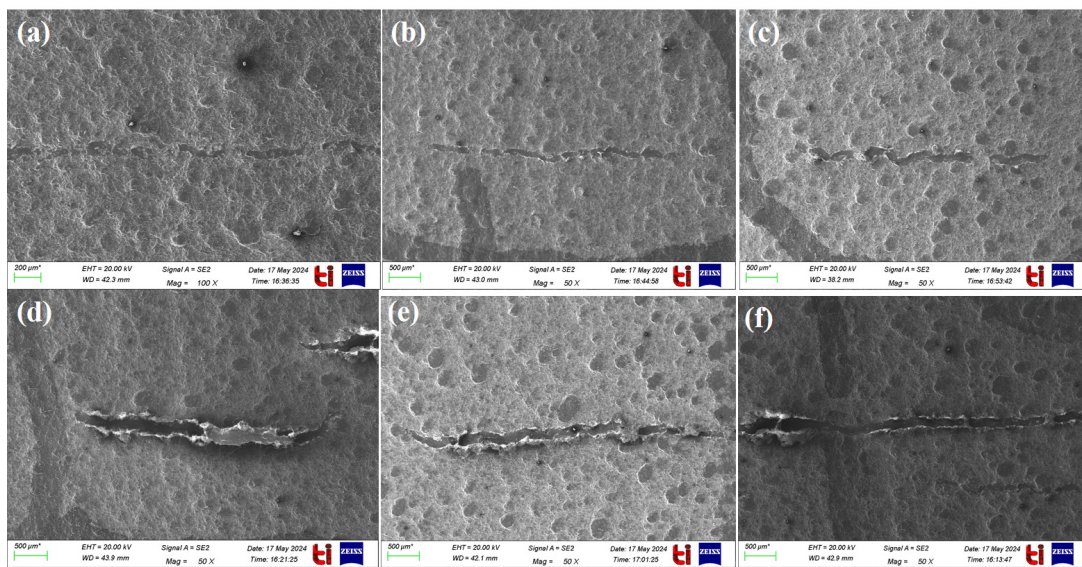


Figure 21: SEM Micrographs of the Al<sub>2</sub>O<sub>3</sub> along with their scratch paths (a) 20N (b) 50N (c) 100N (d) 150N (e) 200N (f) Ramp Load 40-200N

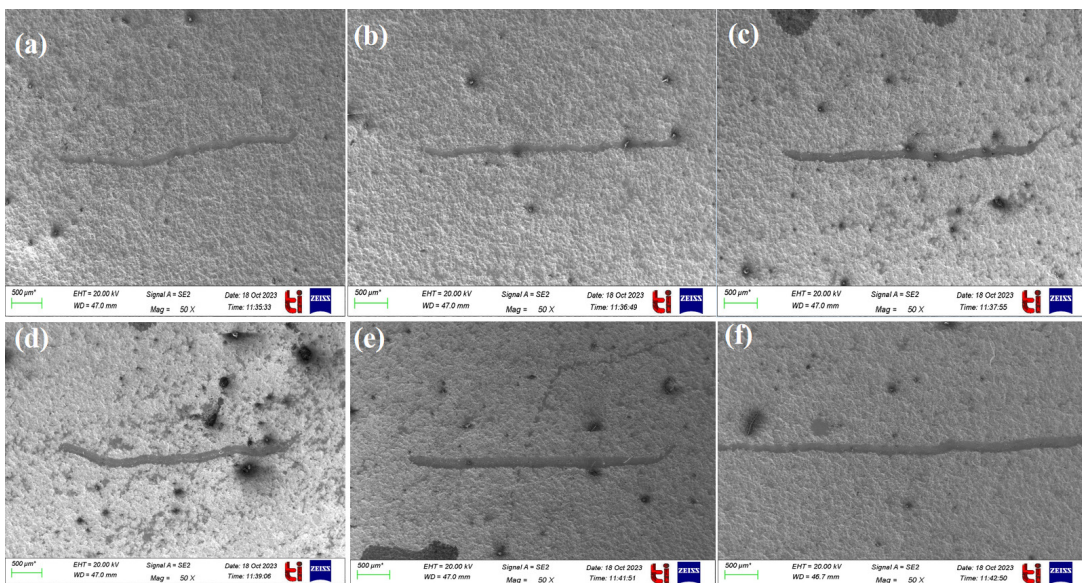


Figure 22: SEM Micrographs of the WC-10Co-4Cr along with their scratch paths (a) 20N (b) 50N (c) 100N (d) 150N (e) 200N (f) Ramp Load 40N-200N

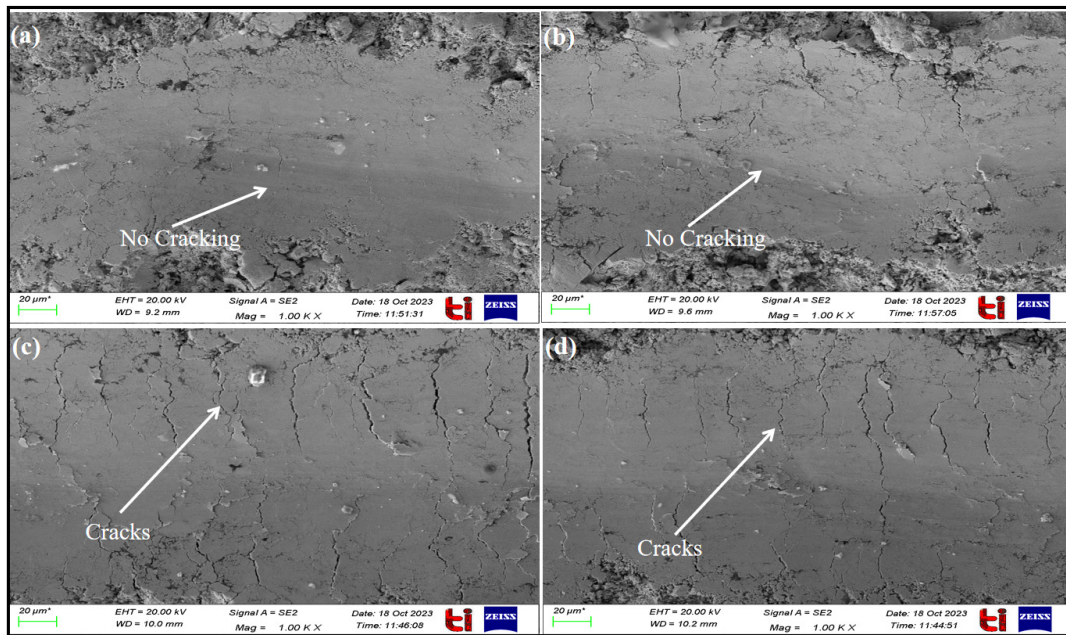


Figure 23: SEM Micrographs of the coating WC-10Co-4Cr at load of (a) 20N (b) 50N (c) 150N (d) 200N

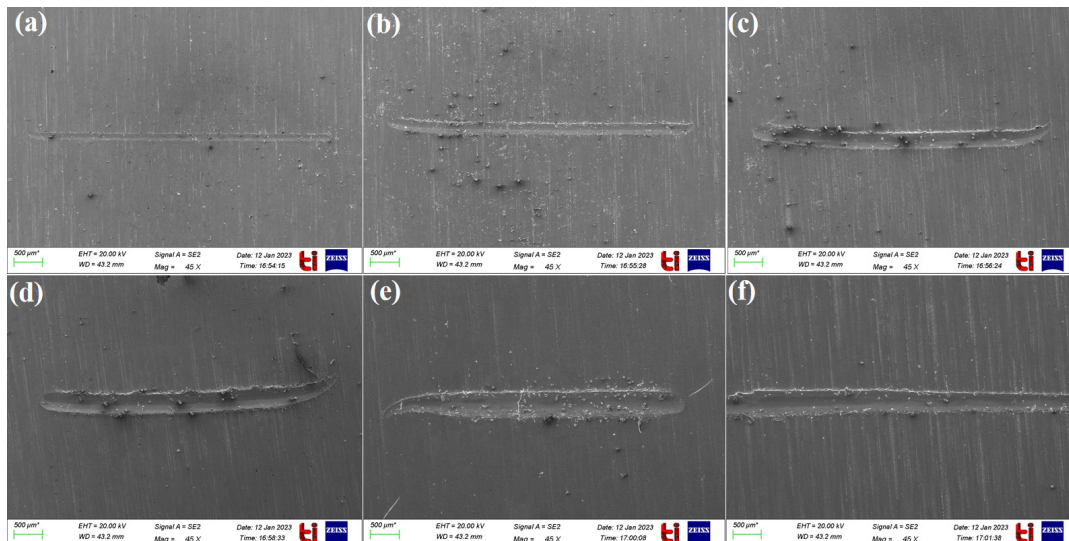


Figure 24: SEM Micrographs of the crack spacing of CA6NM Substrate at load of (a) 20N (b) 50N (c) 100N (d) 150N (e) 200N (f) Ramp Load 20N-200N

Figures 21,22 and 24. For uncoated steel compared to coated steel, the fracture spacing is narrower and more regular regardless of the load.

#### Apparent scratch hardness

Since apparent scratch hardness denotes a material capacity to withstand surface damage from mechanical contact, it is extremely important. Maintaining the robustness, usability, and visual appeal of items depends on this feature. High scratch hardness protects materials from abrasions and scratches, which can degrade the function and look of products including industrial equipment, automobile parts, and consumer electronics. Manufacturers may increase product longevity, save maintenance costs, and improve overall safety and dependability by choosing materials with the right scratch hardness. The crack spacing for Al<sub>2</sub>O<sub>3</sub> coating goes from approximately 125  $\mu\text{m}$  at 20N to a value of 187.50  $\mu\text{m}$  at 200N. A crack spacing of around 105  $\mu\text{m}$  was noted for the

WC-10Co-Cr coated specimen for a load of 20 N and 167  $\mu\text{m}$  for a load of 200N. The crack spacing for an uncoated steel specimen was 133.33  $\mu\text{m}$  at 20N of load and 466.66  $\mu\text{m}$  at 200N of load. Delamination was never seen in specimens with any kind of covering. On the coated specimen, there was some cracking visible in the scratch tracks, and under all weights, a significant pile-up formed along the scratch track's edges.

Apparent scratch hardness', load divided by  $\frac{1}{4}\pi b^4$  (b is the width of the scratch track) is depicted in Table 7, 8 and 9 for the three specimens under investigation. The term "apparent scratch hardness" is used here since it is unknown due to ambiguity in the anticipated load-carrying area. The "real" scratch hardness is defined as the ratio of the load and the load-bearing area [14–16]. Typically, only the front half of the indenter is supported completely by the specimen, but the back half of the indenter may only be

partially supported due to plastic deformation. If the material completely supports the back half of the indenter and there is no piling up in front of the indenter, the apparent scratch hardness and the true scratch hardness are equal [23].

**Table 7:** Apparent scratch hardness vs. load of Al<sub>2</sub>O<sub>3</sub> coated steel

Load (N) (1)	b, Width of the scratch track (μm)	$\frac{1}{4} \pi b^2$ (2)	Apparent Scratch Hardness, GPa = $\frac{(1)}{(2)}$
20N	125	8.78	2.28
50N	133.33	9.07	5.51
100N	152.20	9.69	10.32
150N	166.70	10.14	14.79
200N	187.50	10.76	18.59

**Table 8:** Apparent scratch hardness vs. load of WC-10Co-4Cr coated steel

Load (N) (1)	b, Width of the scratch track (μm)	$\frac{1}{4} \pi b^2$ (2)	Apparent Scratch Hardness, GPa = $\frac{(1)}{(2)}$
20N	105	8.05	2.48
50N	115	8.43	5.93
100N	125	8.78	11.38
150N	136.50	9.18	16.34
200N	167	10.15	19.70

**Table 9:** Apparent scratch hardness vs. load of the uncoated CA6NM specimen

Load (N) (1)	b, Width of the scratch track	$\frac{1}{4} \pi b^2$ (2)	Apparent Scratch Hardness, GPa = $\frac{(1)}{(2)}$
20N	133.33	9.06	2.20
50N	200.00	11.10	4.50
100N	266.66	12.81	7.80
150N	366.66	15.03	9.98
200N	466.66	16.95	11.79

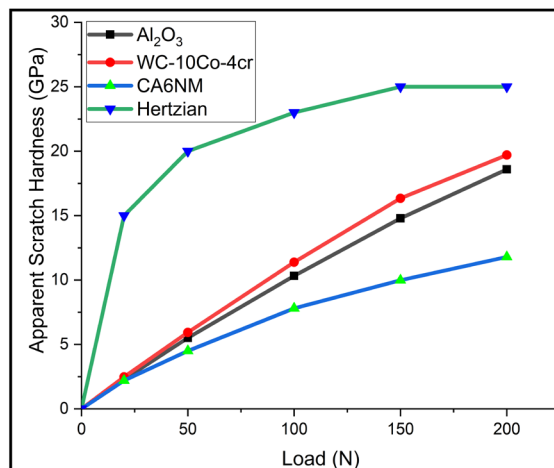


**Figure 25:** Apparent scratch hardness vs. load for the three specimens

Figure 25 demonstrates how coating significantly raises hardness. The hardness of both the coatings Al<sub>2</sub>O<sub>3</sub> and WC-10Co-4Cr has seen a significant modification. The Hertzian solution for an entirely elastic contact is also depicted in figure 25 [23]. The values obtained for the coated specimens match the Hertzian solution for the elastic contact within the bounds of experimental precision. Apart from slight smoothing inside the track, almost no plastic deformation is seen in the alumina and tungsten-coated steel. Ironing is the smoothing process without significant plastic deformation [20]. A clean, sunken track with extensive pile-up at the margin's forms for the uncoated steel. The apparent scratch hardness is, in fact, substantially lower at this stress than the Hertzian solution.

## Conclusions

Based on the results presented above, the following conclusions can be drawn:

1. The powders viz Al<sub>2</sub>O<sub>3</sub>, WC-10Co-4Cr were successfully deposited on the CA6NM steel by D-gun spraying process. Macroscopically, the coatings had smooth surfaces without any visible surface cracks. The steel/coating interface was continuous and well adhered for all the coatings. The apparent porosity of coatings was found to be less than 2 %. The microhardness of the coatings was found to be higher than their corresponding substrates.
2. The material's resistance to scratching was measured by tractional force that offered information on the material's frictional behavior, hardness, and stickiness. The mechanical characteristics of a material were inferred from the plot between force and scratch distance. The tractional force increased with the increase in normal load for all the tested samples. For the coated Al<sub>2</sub>O<sub>3</sub> steel, the tractional force was observed as 7N at 20N normal load, 15N at 50 N normal load, 40N at 100 N normal load and 60N at 150 N normal load.
3. A high coefficient of friction indicates greater resistance to movement, suggesting that the material being scratched is relatively soft or exhibits high friction. Conversely, a low coefficient of friction suggests that the material is hard or has low friction. For all specimens, the friction coefficient rises as the stress rises. The friction coefficient varies depending on the load. The average coefficient of friction value for all loads of Al<sub>2</sub>O<sub>3</sub> coating was 0.193 and the average coefficient of friction value for the WC-10Co-4Cr coated steel for all loads was found to be 0.247. The value of coefficient of friction decreased with the increase in load.
4. WC-10Co-4Cr coating exhibited superior hardness and scratch resistance compared to Al<sub>2</sub>O<sub>3</sub> coating, indicating its potential for applications requiring high wear resistance. WC-10Co-4Cr coating also exhibited consistent scratch resistance across varying loads, indicating its robustness and reliability. Al<sub>2</sub>O<sub>3</sub> coating demonstrated varying levels of scratch resistance under different loads, suggesting potential limitations in applications requiring consistent performance.
5. The apparent scratch hardness of coated and uncoated steel was calculated from the scratch test readings. Scratch test results on coated and uncoated steel were compared, demonstrating that growing coatings made steel harder and more brittle.

6. When the applied force was below the critical value, there was no subsurface damage, but there was plastic deformation and microscopic surface damage. Tensile cracks occurred inside the worn tracks for the coatings when the critical load was exceeded.
7. A material's capacity to withstand wear, distortion, and other types of damage when exposed to abrasive forces may be assessed using the mechanism used in a scratch test.

### Acknowledgement

The authors thankfully acknowledge the SVX Powder M Surface Engineering Pvt. Ltd., Noida, India for providing the D-Gun spray coating service. The authors are highly grateful to the Thapar Institute of Engineering & Technology and Baba Banda Singh Bahadur Engineering College, Fatehgarh Sahib, India for extending the necessary research and testing facility in their premises. The authors also thank IKGPTU Jalandhar, (India) for supporting this work.

### References

1. S. V. Joshi, Sivakumar, Protective coatings by plasma spraying, *Trans. Indian Ceram. Soc.* 50, 50–59 (1991).
2. K. G. Budinski, Surface engineering for wear resistance. Prentice Hall, *Englewood Cliffs* (1988).
3. F. Rastegar, D. E. Richardson, Alternative to chrome: HVOF cermet coatings for high horsepower diesel engines, *Surf. Coat. Technol.* 90, 156–193(1997).
4. B. Rajasekaran, S. G. S. Raman, S. Joshi, G. Sundararajan, Influence of detonation gun sprayed alumina coating on AA 6063 samples under cyclic loading with and without fretting, *Tribol. Int.* 41(4), 315–322(2008).
5. P. M. J. Vuoristo, K. Niemi, T. Mantyla, On the properties of detonation gun sprayed and plasma sprayed ceramic coatings, In Berndt, C.(ed.) *Thermal Spray: International Advances in Coatings Technology*, pp.171–175, ASM International, Metals Park, OH(1992).
6. J. Knapp, Fine-particle slurry wear resistance of selected tungsten carbide thermal spray coatings, *Tribol. Int.* 30(3), 225–234(1997).
7. Y. Liu, T. E. Fischer, A. Dent, Comparison of HVOF and plasma-sprayed alumina/ titania coatings—microstructure, mechanical properties and abrasion behavior, *Surf. Coat. Technol.* 167, 68–76(2003).
8. P. P. Psyllaki, M. Jeandin, D.I. Pantelis, Microstructure and wear mechanisms of thermal-sprayed alumina, *Coat. Mater. Lett.* 47,77–82(2001).
9. J. Voyer, B. R. Marple, Sliding wear behavior of high velocity oxy-fuel and high power plasma spray-processed tungsten carbide-based cermet coatings, *Wear* 225–229,135–145(1999).
10. Y. Wang, Friction and wear performances of detonation-gun and plasma-sprayed ceramic and cermet hard coatings under dry friction, *Wear* 161,69–78(1993)
11. L. Pawlowski, *The Science and Engineering of Thermal Spray Coatings*, Wiley, West Sussex P109 IUD (1995).
12. S. Guessasma, M. Bounaze, P. Nardin, T. Sahraoui, Wear behavior of alumina–titania coatings: analysis of process and parameters, *Ceram. Int.* 32,13–19(2006).
13. M.G. Gee, C. Phatak, R. Darling, Determination of wear mechanisms by stepwise erosion and stereological analysis, *Wear* 258(2004)412–425.
14. J.A. Williams, *Tribol. Int.* 29(1996)675–694.
15. B.J. Briscoe, P.D. Evans, E. Pelillo, S.K. Sinha, *Wear* 200(1996)137–147.
16. V. Testa, S. Morelli, G. Bolelli, B. Benedetti, P. Puddu, P. Sassatelli and L. Lusvarghi, Alternative metallic matrices for WC-based HVOF coatings, *Surface and Coatings Technology*, Volume 402(2020),126308.
17. P.H. Shipway and L. Howell, Microscale abrasion–corrosion behaviour of WC–Co hardmetals and HVOF sprayed coatings, *Wear*, 258, 1–4(2005),303–312.
18. J. Perry, Scratch adhesion testing of hard coatings, *Thin Solid Films*, Volume 107, Issue 2,1983, 167–180,ISSN 0040-6090,https://doi.org/10.1016/0040-6090(83)90019-6.
19. Yinglong Wang, Stephen M. Hsu, Lubricated friction and wear simulation of multi-scratches in asperity-asperity contact, *Wear*, 217, 1,1998, 104–109.
20. Gidla Vinay, Ravi Kant, Harpreet Singh, Influence of powder heat treatment and particle size on the corrosion performance of cold-sprayed nickel-aluminum bronze (NAB) for repair applications, *Corrosion Science*, 238,2024,112355.
21. J.L. Bucaille, E. Felder, G. Hochstetter, *Wear* 249(2001)422–432.
22. J. D. Kamminga, P. F. A. Alkemade and G. C. A. M. Janssen, Scratch test analysis of coated and uncoated nitrided steel, *Surface and Coatings Technology* 177 – 178(2004)284–288
23. G.M. Hamilton, *Proc. Inst. Mech. Eng.* 197C (1983) 53–5
24. Briscoe, B., Pelillo, E., Ragazzi, F., & Sinha, S. (1997). Scratch deformation of methanol plasticized poly(methylmethacrylate) surfaces. *Polymer*, 39(11), 2161–2168.

